

# We are IntechOpen, the world's leading publisher of Open Access books Built by scientists, for scientists

6,900

Open access books available

186,000

International authors and editors

200M

Downloads

Our authors are among the

154

Countries delivered to

TOP 1%

most cited scientists

12.2%

Contributors from top 500 universities



WEB OF SCIENCE™

Selection of our books indexed in the Book Citation Index  
in Web of Science™ Core Collection (BKCI)

Interested in publishing with us?  
Contact [book.department@intechopen.com](mailto:book.department@intechopen.com)

Numbers displayed above are based on latest data collected.  
For more information visit [www.intechopen.com](http://www.intechopen.com)



## Chapter

# Carbon Soot Polymer Nanocomposites (CSPNCs): Production, Surface Morphological, Glass Transition Temperature Phenomenon and Optical Properties

*Rakhi Tailor, Yogesh Kumar Vijay and Minal Bafna*

## Abstract

The present chapter covers the production and properties of carbon soot nanoparticles (CSNPCs) and their doped carbon soot polymer nanocomposites (CSPNCs). The first part of this chapter will provide a brief introduction of carbon soot, its morphology, production and synthesis methods. The second part will explain the investigation of carbon soot nanoparticles by flame deposition method and their properties. The third part will provide a short knowledge on polymer nanocomposites (PNCs) and their processing methods. The last part will illustrate the production of carbon soot polymer nanocomposites by solution casting method and their important properties. At the end, the chapter concludes with future scopes.

**Keywords:** carbon soot (CS), carbon soot polymer nanocomposites (CSPNCs), almond soot (AS), mustard soot (MS), energy band gap ( $E_g$ )

## 1. Introduction

Carbon particulate matters are small spherical particles in the range between 100 and 500 Å of diameter and synthesized by the combustion process [1, 2]. We will study these spherical particles by means of electron microscopy. X-ray diffraction technique (XRD) reveals that each soot particle contains thousands of crystallites and carbon sheet atoms with the graphite structure [3]. Researchers observed that the soot particles are aggregates of a number of tiny spherical particles, named primary particles [4, 5]. The chemical study of soot particles reveals that these particles are composed of elements other than just carbon. Carbon soot particles are composed of 1% hydrogen [1, 2] and up to 3% in weight of polycyclic organic matter [6]. In 1960, Lindsay collected soot samples by the combustion of 16 different hydrocarbons and extracted them with cyclohexane [7]. Carbon soot has several kinds of sources such as burning of oils, biomass fuels or any deliberate fires. The investigation of soot in a flame is a complete process, composed of

many mechanisms, and it depends on the composition of fuels [8]. In 1984, Melton suggested that carbon soot is an insoluble solid substance and roughly consists of eight carbon atoms and a single hydrogen atom [9]. Joyce found that soot is hard amorphous carbon particles in microscopic size [10]. Researchers found that soot particles are small in size but spherical hard particles in the range of 10–35 nm. These nanoparticles basically consist of carbon atoms arising from the fuel combustion at high temperature with a condition when the oxygen amount is insufficient to convert all the fuel in to CO<sub>2</sub> and H<sub>2</sub>O [11, 12]. Soot particles can aggregate in soft and slippery secondary particles by their structure of agglomeration having average size of 120 nm or greater than 400 nm [13, 14].

## **2. Carbon soot**

### **2.1 Carbon soot morphology**

The structure of soot is difficult to define to a properly satisfactory extent. Soot obtain from combustion process and pyrolysis of hydrocarbons are composed of primary spheres agglomeration with a range of 10–15 nm in a diameter for a broad type of operation conditions [15].

The distribution of size mainly depends upon the primary spheres. Some researchers recorded that mustard soot has parallel physical and chemical characteristics to form the different types of soot, and it has been found that the primary particles could be as small as in a diameter [16].

Morphology of carbon soot particles from different field flames have been carried out using scanning electron microscopy (SEM) and transmission electron microscopy (TEM). The primary particles are composed of agglomerates like chain of individual spheres [17, 18]. The internal structure of soot particles is analyzed by high-resolution phase contrast electron microscopy [19].

According to the chemical study of soot, carbon is a main component in soot, but hydrogen and minor constituents can be present. The carbon hydrogen mole ratio of premature soot particles (primary soot particles) obtained by hydrocarbon fuels is equal to one or less than one, but this ratio for mature soot particles (aggregate soot particles) is high or approximately equal to 10 as compared to premature (C/H) ratio [18]. Agglomerated particles produced by the combustion method have been found to be in the range of 100 nm to 2 μm [20, 21]. The nanosize of soot particles is dependent on various conditions such as the production of sampling, operations and type of fuels. The term nanostructure of the soot is used to characterize the graphene layer plane dimensions its relative orientation and tortuosity [22, 23].

### **2.2 Production and destruction method of soot**

Soot particles basically consist of carbon, oxygen and hydrogen, and some other constituents such as nitrogen, zinc, sulfur, etc. are also observed [24, 25]. In **Table 1**, the typical composition of soot obtained from the lubricant oil and soot contained are shown [26]. Soot in individual particles or spherical agglomerates is composed of many primary particles with approximately 10–50 nm in diameter [27]. The size of soot particles increases due to agglomeration because some particle diameters are up to 200 nm, and in this process, the soot-free radical character decreases.

The formation of soot is a complex process because this involves several physical and chemical steps and is still regarded as only partially understood. Soot particles

Soot composition	Soot content (%)
Carbon	90
Oxygen	4
Volatile content	6

**Table 1.**  
*Soot percentage composition.*

obtained from different sources such as various fuels and combustion are expected to be approximately similar in composition and size, suggesting the same processes of formation and growth constraints. Many authors have presented a model of soot formation from liquid or vapor phase combustion, which mainly comprises or is classified in to five distinct and normal identified processes, namely pyrolysis, nucleation, surface growth, coalescence and agglomeration as presented in **Figure 1** [18, 28, 29].

Carbon soot production is also visualized as being a fuel thermal stability function [30]. Some authors also investigated that in the pyrolysis all hydrocarbons yield acetylene, which is the most precursor of species by incomplete combustion [31–33]. This is contributed to its low thermal stability where it easily breaks in to carbon solid and hydrogen. A well-defined and accepted theory for the formation of soot is explained by Haynes [18].

### 2.3 Investigation of carbon soot nanoparticles

Carbon nanosoots have been produced by two different edible oils by flame deposition techniques in two different environments.

#### 2.3.1 Formation of soots in natural environment (without water tub)

At room temperature, the flame deposition method is a well known, cost-effective and easiest method to produce carbon nanosoot from different oils (**Figure 2**). In this technique, we take two diyas or “clay lamp”: one filled with almond oil and the other one is filled with mustard oil. Dip a cotton wick in both diyas and put it on the floor at some distance (approx. 40 cm). Light up cotton wick. To collect carbon soot particles, put another diya in reverse at some height with the help of other layers of diyas and make the arrangement.

In this arrangement, the distance between the tip of the wick and collector diyas' surface is approximately 5 cm. The distance has been optimized by carrying out the pyrolysis process at various source collector distances. The flame stabilizes after 1–2 min and then the almond oil soot and mustard oil soot are allowed to deposit on the collector. For 2 h, the almond and mustard oils were burned, and then the generated soots were scrapped off using a spatula on butter paper and then samples were packed in air-tight bottles with proper labeling.

#### 2.3.2 Formation of soots in water tub environment (with water tub)

In this section, the procedure of soot production from almond and mustard oil at a room temperature is the same as above mentioned (see Section 2.4.1). The only change made in this section is to introduce a water tub. The entire setup is arranged in a water tub to provide the sample surroundings extra moisture (**Figure 3**). After completion of the processes, all soot samples were stored in air-tight bottles and labeled (**Figure 4**).

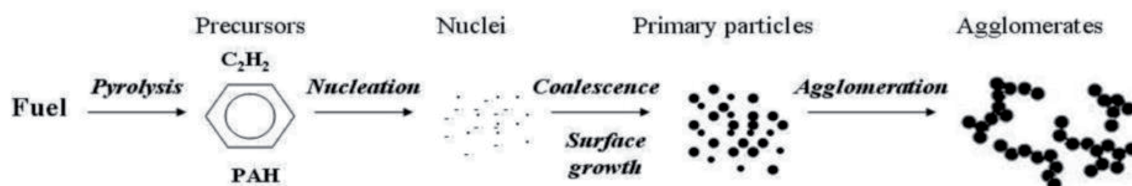


**Figure 1.**  
Soot formation steps from fuel.



**Figure 2.**  
Carbon soot-producing setup in natural environment.

## 2.4 Properties of carbon soot nanoparticles (CSNPCs)

### 2.4.1 X-ray diffraction analysis of almond soot (AS) and mustard soot (MS) nanoparticles

#### 2.4.1.1 XRD analysis of almond oil soots

The X-ray diffraction spectra in **Figure 5** are from almond soot without and with water tub environment. Samples show carbonaceous soot. The two theta values at 24.74 and 42.13° are identified for natural environment (without water tub) as graphite peaks. These peaks correspond to plane (002) and (101), respectively. Similarly, the sample with water tub got two prominent peaks. A high-intense peak at 24.04° and a low-intense peak at 43.69° appeared. As shown in the figure, the peaks of samples in the presence of water tub are with greater intensities as compared to samples in natural environment. Due to this property, its crystallinity is not lost. A high-intense peak at 24.74 and 24.04° for natural and with water tub soot indicates the presence of large amount of amorphous carbon. Two peaks are at 42.13 and 43.69° and indicate the presence of low-quality carbon nanomaterial. All these peaks denote the presence of multiwalled graphite carbon nanotubes.

#### 2.4.1.2 XRD analysis of mustard oil soots

The XRD profiles of carbon soot that are obtained without and with water tub (**Figure 6**), respectively, are quite similar in their pattern, both showing two



**Figure 3.**  
*Carbon soot-producing setup in water tub environment.*



**Figure 4.**  
*Picture of generated soot samples for characterization.*

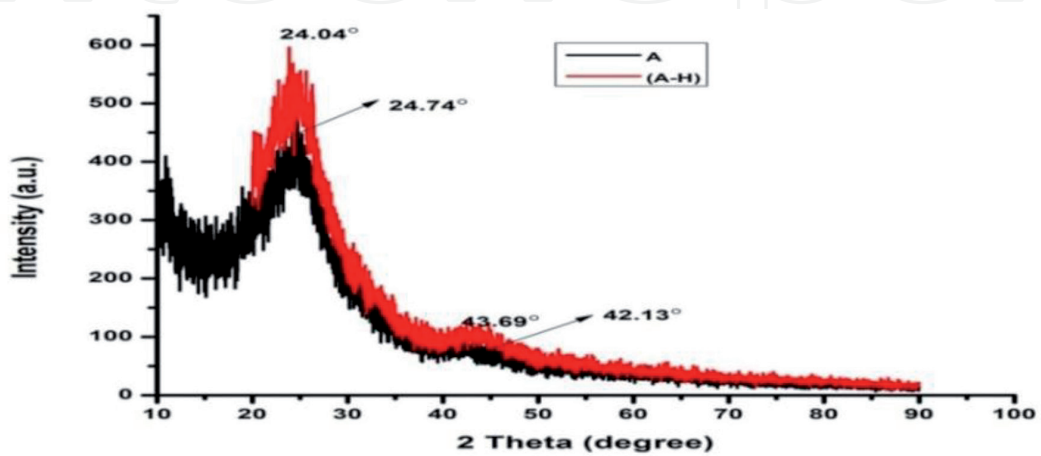


**Figure 5.**  
*XRD spectra of almond soot without (A) and with water tub (A-H) environment.*

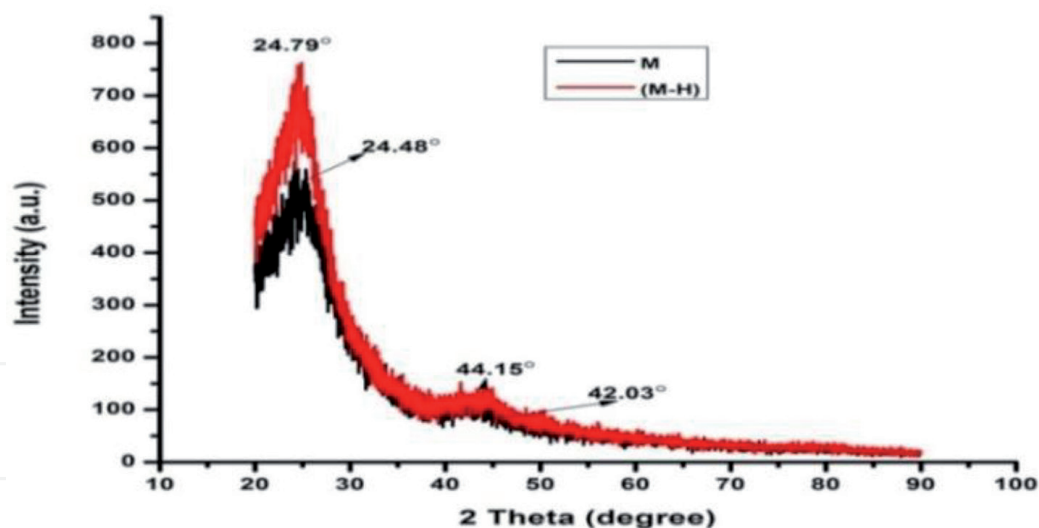


**Figure 6.**  
XRD patterns of mustard soot without (M) and with water tub (M-H) environment.

prominent broad diffused peaks. The sample with water tub exhibits higher intensity suggesting that the surrounding of water or creation of humid environment makes it less amorphous. For the soot samples without water tub, high-intense Bragg diffraction peak is found at  $2\theta = 24.78^\circ$  and a low-intense peak at  $44.15^\circ$  for (002) and (100) reflections, respectively. These reflections suggest that the soots obtained by this method have a good extend to layer formation. Similarly, in the case of soot sample with water tub, a high-intense peak at  $24.48^\circ$  and low-intense peak at  $42.03^\circ$  show that crystallinity is not lost due to oxidative acid treatment, and these two peaks at  $24.48^\circ$  and  $24.70^\circ$  are a high-intensity broad peak, which indicates the presence of large amount of amorphous material in the soots. The low-intensity peaks at  $42.03^\circ$  and  $44.15^\circ$  are an indication of the low quality of carbon nanoparticles present in soots with and without water tub, respectively, and these observations are in quite agreement with the result reported by other researchers [34, 35].

#### 2.4.2 Field emission scanning electron microscopy analysis of almond soot (AS) and mustard soot (MS) nanoparticles

##### 2.4.2.1 Field emission scanning electron microscopy analysis of almond oil soots

The almond soot material deposited on glass surface was investigated by scanning electron microscopy for without and with water tub conditions. The particles are very small occurring nonindividually and individually. Synthesized soot particles in flame deposition method break up to form other small substances. For the first condition, surface morphology is seen to be nonuniform (**Figure 7a**), and there are several grains that look like carbon nanotubes, but for the second condition, it is seen to be uniform and particle size is small comparatively (**Figure 7b**). The SEM images for both conditions show carbon soot particles of average size approximately 50 nm. The formed soot particles show morphology of agglomerated clusters for without water tub sample and uniformly distributed carbon nanoparticles for with water tub sample.

##### 2.4.2.2 FESEM analysis of mustard oil soots

Mustard oil is burned in two different environment to obtain soot by a flame deposition process in which oil breaks up to form other substances. The SEM images

of obtained particles describe the synthesized carbonaceous particles from burning of oil and are a mixture of elemental carbon and oxygen, a variety of hydrocarbons. The surface morphology of the deposited carbon obtained is seen to be nondistinguishable in natural environment sample (**Figure 8a**) and distinguishable in water tub environment sample (**Figure 8b**).

The prepared soot particles are agglomerated in a range between 50 and 100 nm, but most particles are about 50 nm in size. As shown in all SEM images, agglomerated soot particles with well-defined boundaries are arranged in the form of a chain (carbon necklace).

### 2.4.3 Chemical composition analysis of almond soot (AS) and mustard soot (MS) nanoparticles

#### 2.4.3.1 Energy dispersive X-ray study of almond oil soots

Energy dispersive X-ray of almond oil soot particles is presented for natural and with water tub condition. The spectra show the presence of carbon and oxygen. For the first condition (**Figure 9a**), the EDAX analysis indicates the soot to consist 92.10% weight of carbon and 7.9% weight of oxygen. For the second condition (**Figure 9b**), it consists of 87.86% carbon and 12.14% weight of oxygen. **Table 2** shows the percentage composition of elements carbon and oxygen obtained from

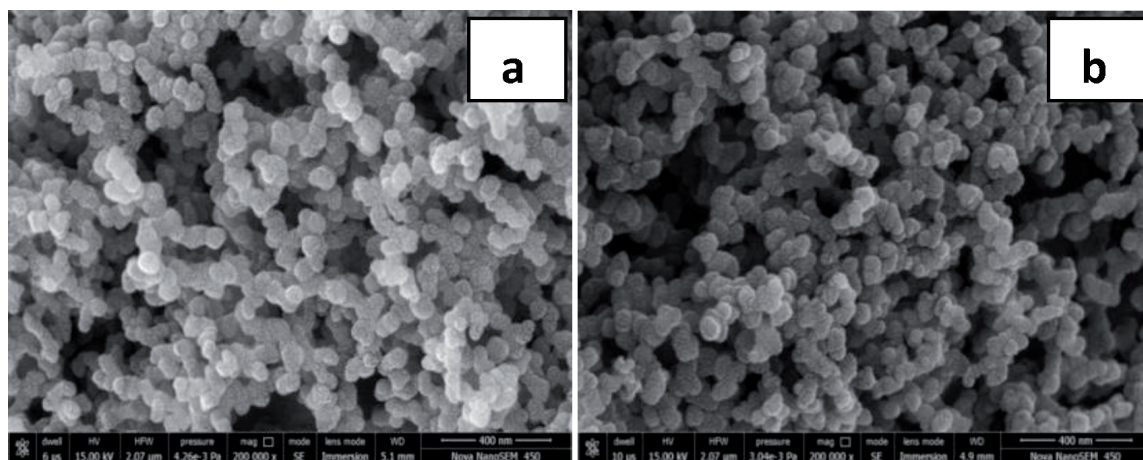


**Figure 7.** Field emission scanning electron micrograph of almond oil soot (a) natural environment and (b) with presence of water tub.

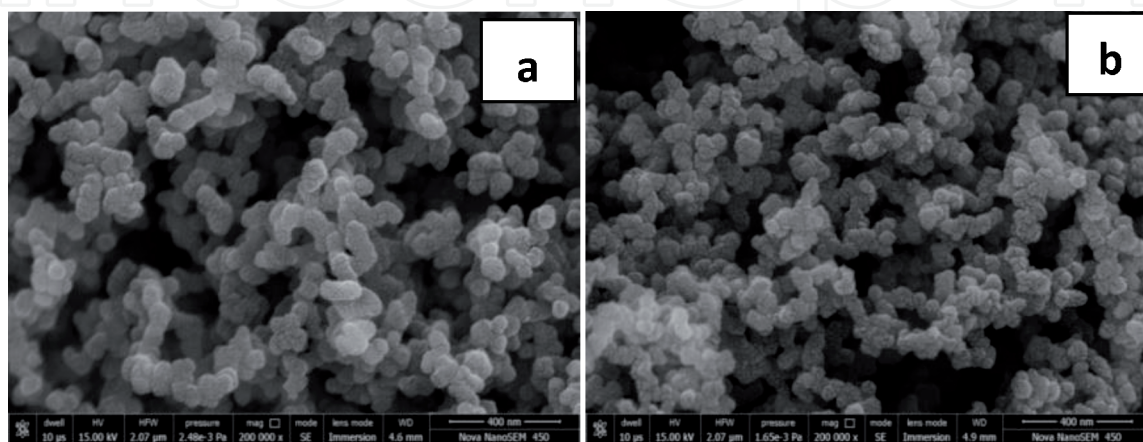


**Figure 8.** Field emission scanning electron micrograph of mustard oil soot (a) natural environment and (b) with presence of water tub.

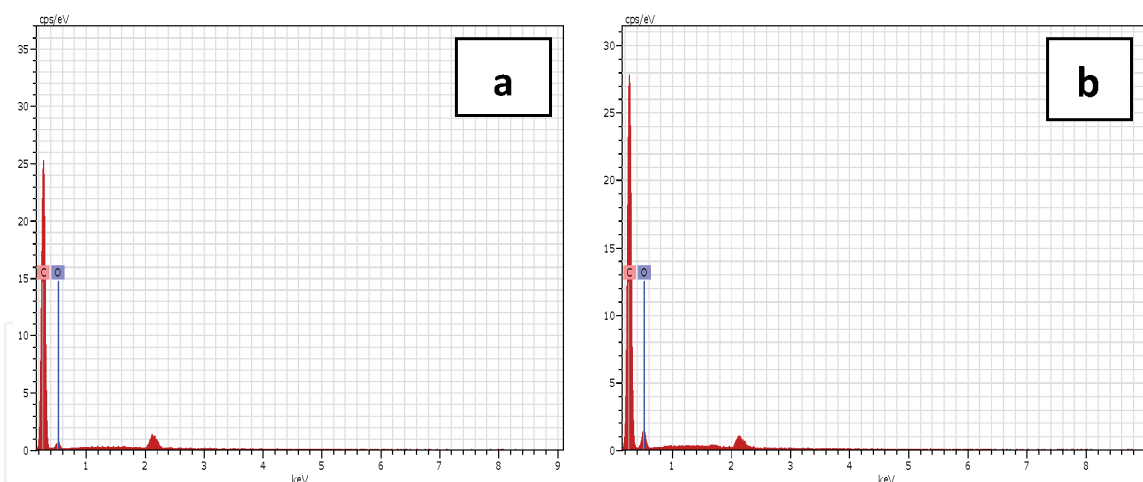


**Figure 9.** EDAX spectra of almond oil soot in (a) without and (b) with water tub environment.

Samples of soot particles	Percentage of carbon and oxygen elements	
	Carbon element (C%)	Oxygen element (O%)
Almond oil soot without water tub	92.10	7.90
Almond oil soot with water tub	87.86	12.14
Mustard oil soot without water tub	83.37	16.63
Mustard oil soot with water tub	90.81	9.19

**Table 2.** Elemental composition of almond and mustard oil soot in natural and with water tub environment.

EDAX spectra of different samples in different conditions. The spectra reveal that almost 85% of the sample contains pure carbon and remaining 15% oxygen, confirming the absence of any other external impurities. This AS sample is electrically nonconducting, and for EDAX analysis, this sample is coated with gold to convert it into electrically conducting. Due to of this, an extra small peak is observed for gold at approximately 2 keV in EDAX spectra.

#### 2.4.3.2 EDAX study of mustard oil soots

The elemental analysis of synthesized mustard soot was performed using energy dispersive X-ray (EDAX). The spectra show the presence of carbon and oxygen for both conditions. The composition of soot aggregates from the EDAX analysis shows the soot to consist of about 83.37% weight of carbon and 16.63% weight of oxygen element for first condition (**Figure 10a**), and similarly for second condition (**Figure 10b**), it consists of about 90.81% weight of carbon and 9.19% weight of oxygen as shown in **Table 2**. The result shows the product of the flame deposition of mustard oil to be composed of mainly almost (80–90)% carbon and remaining (10–20)% oxygen.

The EDAX of soot samples indicates the presence of no other except carbon and oxygen. This MS sample is electrically nonconducting, and for EDAX analysis, this sample is coated with gold to convert it into electrically conducting. Due to of this, an extra small peak is observed for gold at approximately 2 keV in EDAX spectra.

#### 2.4.4 Fourier transform infrared spectroscopy analysis of almond soot (AS) and mustard soot (MS) nanoparticles

##### 2.4.4.1 Fourier transfer infrared analysis of almond oil soots

FTIR transmission spectra for without and with water tub samples are shown in **Figure 11**.

A peak at  $3435\text{ cm}^{-1}$  is for water O–H stretch, peaks at  $2918$  and  $2919\text{ cm}^{-1}$  are for C–H stretch or carboxylic acid O–H, and peaks at  $2850\text{ cm}^{-1}$  are for C–H stretch or (–C–H) aldehyde. A weak peak for both soot spectra at  $1617\text{ cm}^{-1}$  is detected for C=C aromatic stretch. Two bands are at  $1384$  and  $1377\text{ cm}^{-1}$  stretch for –CH<sub>3</sub> group. Some detected bands at low wave numbers  $1048$ ,  $668\text{ cm}^{-1}$  and  $1047$ ,  $705\text{ cm}^{-1}$  indicate the presence of SP<sup>2</sup> and SP<sup>3</sup> aromatic clusters of amorphous carbon soot.

##### 2.4.4.2 FTIR analysis of mustard oil soots

FTIR spectroscopy analysis was carried out to identify the chemical structure of carbon soot nanoparticles as well as the presence of any functional group, and the obtained spectra are shown in **Figure 12**, respectively.

FTIR spectra of Mustard Oil soot without and with water tub environment conditions, shows that in between  $1500$  to  $4000\text{ cm}^{-1}$  range spectra resemble in their profile and full spectra remain in the range  $400$  to  $4000\text{ cm}^{-1}$ .

The broad vibration band at  $3435\text{ cm}^{-1}$  is attributed to the OH stretching of the carboxylic acid group. It also indicates the presence of absorbed moisture of OH group in the samples, and it is therefore more intense for with water tub sample as compared to without water tub as expected. Another vibration band at  $2919$  and  $2852\text{ cm}^{-1}$  is due to symmetric and antisymmetric C–H bond stretching. The band at  $1725\text{ cm}^{-1}$  is assigned to C=O stretching vibration associated with the presence of carboxylic acid group. A band centered at  $1619\text{ cm}^{-1}$  with a shoulder at  $1384\text{ cm}^{-1}$  may be due to (C=C) stretching vibrations. A band at  $1217\text{ cm}^{-1}$  is associated with CO stretching vibrations. A band centered at  $1047\text{ cm}^{-1}$  corresponds to C–N stretch. Some obtained bands at low wave numbers  $826$ ,  $738$  and  $597\text{ cm}^{-1}$  indicate the presence of small (SP<sup>2</sup> and SP<sup>3</sup>) clusters.

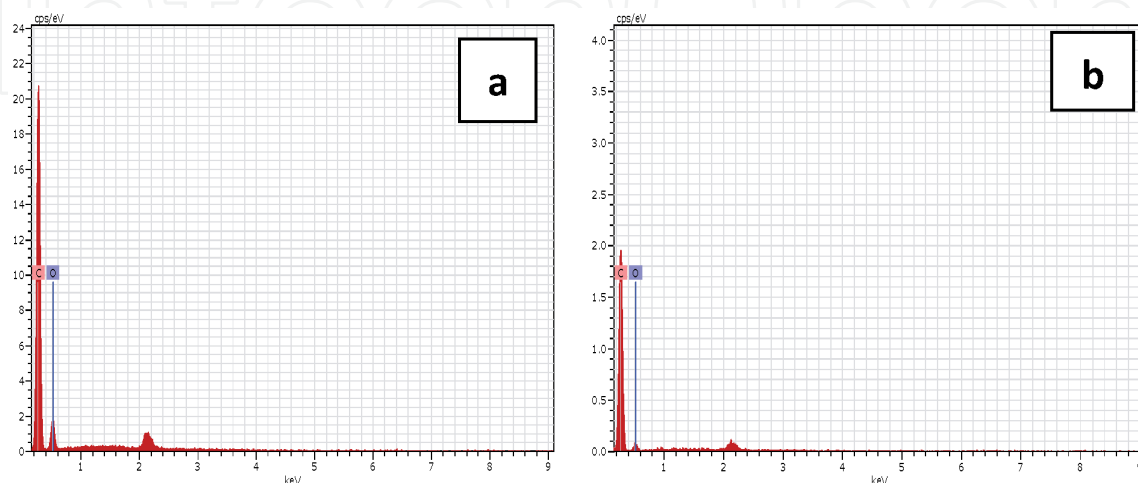


**Figure 10.**  
EDAX spectra of mustard oil soot in (a) without and (b) with water tub environment.

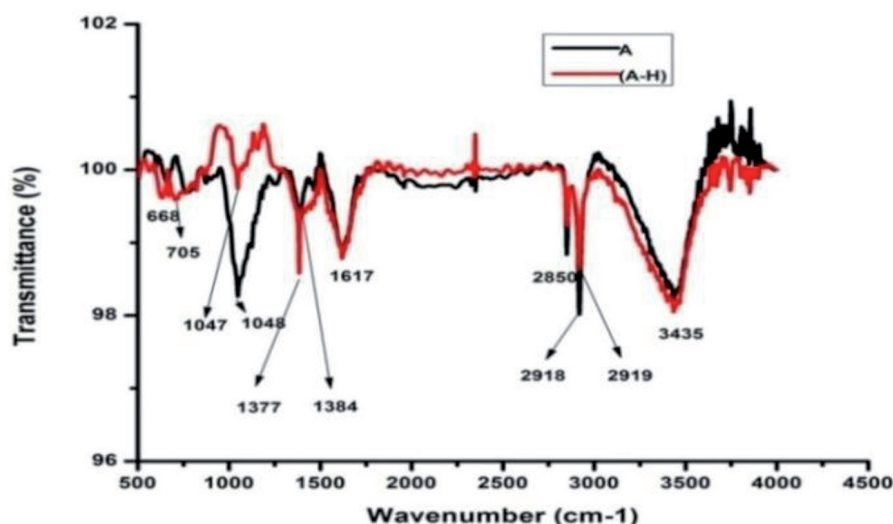


**Figure 11.**  
FTIR spectra of almond soot in without (A) and with water tub (A-H) environment.

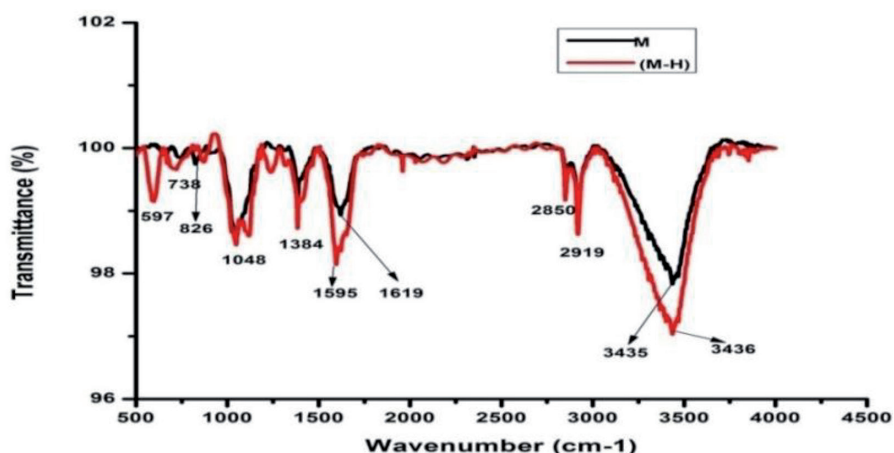


**Figure 12.**  
FTIR spectra of mustard oil soot in without (M) and with water tub (M-H) environment.

These observations are in good agreement with the earlier reported ones [35–37]. So the IR studies directly prove the presence of carboxylic acid groups and clusters in synthesized soot.

### 3. Polymer nanocomposites (PNCs)

The nanomaterials can be divided into two types: one is nanostructured materials and another one is nanophase materials. Normally, bulk materials are made by grains (agglomerates) with the nanometer range. Nanocomposites refer to materials existing of minimum two phases with one dispersed in another and making a 3D network. The dispersion medium is called matrix and the dispersed phase is called filler. If the host matrix of nanocomposite is polymer, then the resulting nanocomposite is called polymer nanocomposite (PNC). PNC belongs to the nanostructural class material. If filler has higher dimensions, the resulting composite refers to polymer composite (PC). PNCs are different to other PC materials; their filler consists at the nanoscale [38, 39]. According via, PNC's particles exists on nanoscale measure and particles with nanoscale arrangements has a polymer host matrix with nanoparticles. PNCs have been shown to possess the classic thermal and mechanical

properties [40, 41]. Nanoparticles are in size less than the wavelength of visible light, giving the unique optical properties.

#### 4. Production of carbon soot (AS and MS)/PMMA nanocomposites

The synthesizing technique in the production of carbon soot polymer nanocomposites was a mixture of solution mixing and solvent casting. In this section, synthesized nanocomposites for two different nanofillers are discussed: one is AS/PMMA nanocomposite and the other one is MS/PMMA nanocomposites.

- For the solution of PMMA, PMMA was dissolved in 20 ml dichloromethane (DCM) solvent using the help of magnetic stirrer for a duration of 3 h (Figure 13).
- Nanofiller carbon soots (almond soot particles and mustard soot particles) 1 and 2 mg were dispersed in the polymer solution by ultrasonication for 4 h



**Figure 13.**  
*Actual setup of pure PMMA solution by magnetic stirrer and ultrasonication.*



**Figure 14.**  
*Actual setup of CS/PMMA homogeneous solution by magnetic stirrer and ultrasonication.*

(at the end temperature of sonication was 35°C) to get a homogeneous solution (**Figure 14**).

- At the end, a homogeneous solution was purged in a flat glass Petri dish, which was floating over mercury in vacuum box.
- We take the prepared homogeneous solution for approximately 24 hr in a Petri dish in low vacuum (8-10mTorr) at room temperature, and after the thin film samples reach a dry state, they are removed from Petri dishes.
- Thin film of polymer (PMMA) without the nanofiller (carbon soots) was also prepared for the reference composite used in the comparison study of many composite properties. The film of pure PMMA was transparent and other composite films were opaque and in black color due to dispersion of carbon soots. All produced films were in the thickness of 100  $\mu\text{m}$  for pure PMMA and different concentration (1 and 2 mg) of carbon soot nanofillers.

## 5. Properties of CS/PMMA nanocomposites (CSPNCs)

### 5.1 Surface morphological and chemical composition properties

Atomic force microscopy study is a characteristic and quantitative analysis for measuring the surface roughness at nanodimension and visualizing the nanotexture of the deposited thin film surface. The topography deflection image and 3D AFM images of the pure PMMA and CS/PMMA nanocomposites, in which the roughness value of nanocomposites are carried out, are shown in **Figure 15a–c**.

The roughness parameter with average roughness ( $R_a$ ), root mean square roughness ( $R_q$ ), skewness of the line ( $R_{sk}$ ) and kurtosis of the line ( $R_{ku}$ ) roughness data are shown in **Table 3**. The pure PMMA thin film, AS/PMMA and MS/PMMA thin films are synthesized for comparative analysis of surface roughness. The measures of roughness of carbon soot polymer thin films are less than the roughness of pure PMMA film. This implies that the prepared PMMA thin films with almond and mustard soot decrease the surface roughness. The ration of roughness value  $R_q$  and  $R_a$  ( $R_q/R_a$ ) are approximately close to theoretical data, recorded by Ward et al. in 1982 [42].

The chemical composition for CSPNCs was carried out by EDAX (energy dispersive X-ray analysis). Results from EDAX depicted in **Figure 16a–c** reveal the chemical composition as follows:

Carbon approximately 75% and remaining oxygen approximately 25% for all nanocomposite samples with individual content of PMMA, AS/PMMA and MS/PMMA are 76.31, 76.20, 75.26% and 23.69, 23.80, 24.74% respectively (**Table 4**). These CS (AS and MS)/PMMA samples are electrically nonconducting, and for EDAX analysis, these samples are coated with gold to convert them into electrically conducting. Due to this, an extra small peak is observed for gold at approximately 2 keV in EDAX spectra.

### 5.2 Spectroscopic properties

The FTIR spectra of PMMA show sharp intense peaks at 1725 and 1141  $\text{cm}^{-1}$  and are attributed to the ester carbonyl stretching and C–O–C bending vibration. In addition, peaks appeared at 3000 and 2950  $\text{cm}^{-1}$  and are assigned to the C–H stretching vibrations, while the peaks at 752 and 840  $\text{cm}^{-1}$  are attributed to the

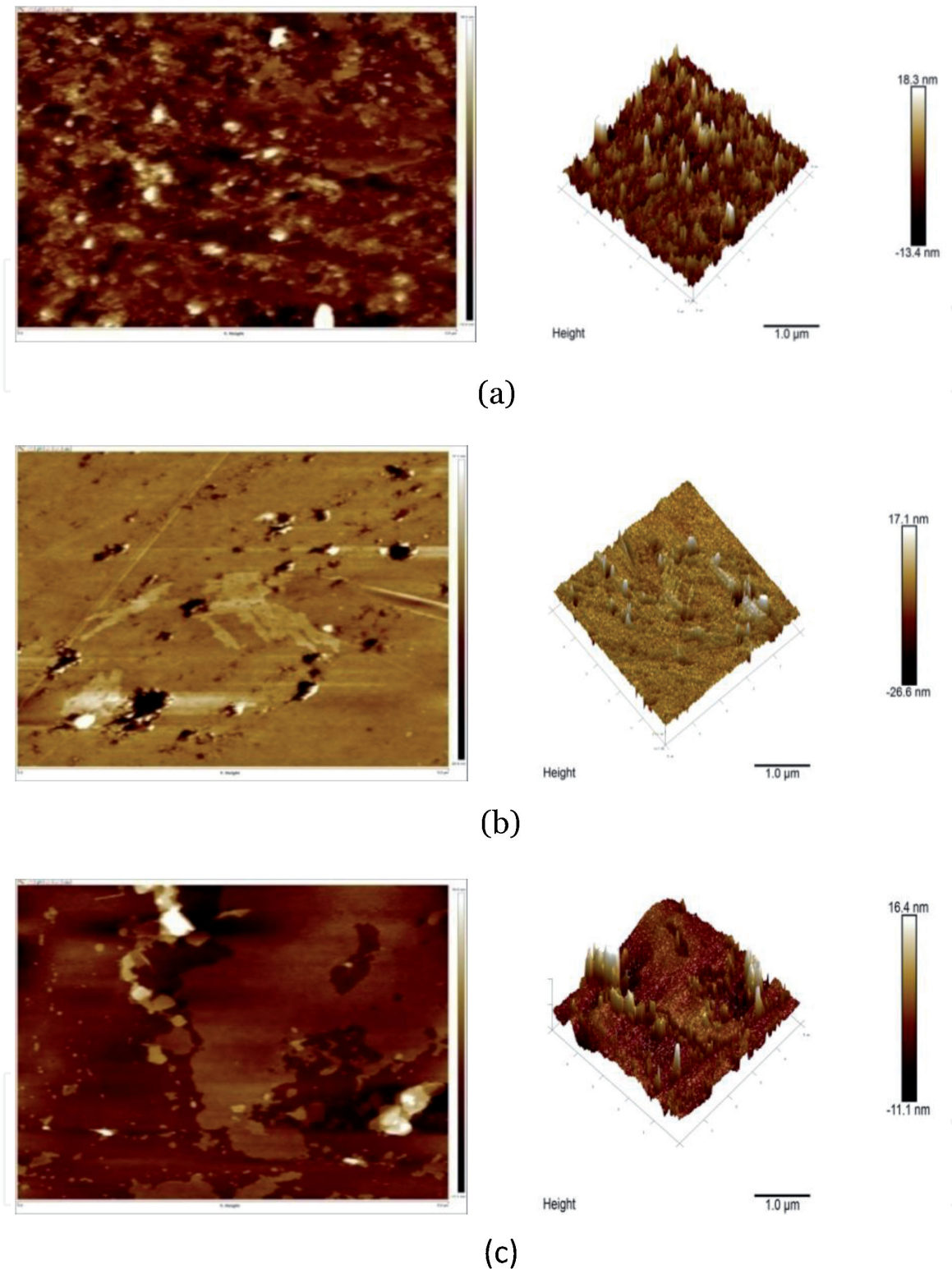


**Figure 15.** Topographic deflection image and 3D image of (a) pure PMMA, (b) AS/PMMA, and (c) MS/PMMA thin film.

vibration of polymethyl methacrylate chains and the deformation vibration of PMMA O–C–O, respectively. Moreover, the peaks at 1236, 1383 and 1440  $\text{cm}^{-1}$  were attributed to the ester band symmetrical and asymmetrical stretching vibrations. The peak at 984  $\text{cm}^{-1}$  represented C–H bending wagging vibration. It should be noted that there is no peak near 1680 to 1640  $\text{cm}^{-1}$  range, which confirms that all methyl methacrylate (MMA) monomers are converted into PMMA polymer. The FTIR patterns of almond soot-doped PMMA viz. pure and mustard soot-doped PMMA viz. pure are shown in **Figures 17** and **18**, respectively.

Samples	Roughness parameters				
	$R_a$ (nm)	$R_q$ (nm)	$R_q/R_a$	$R_{sk}$	$R_{ku}$
Pure PMMA	2.99	4.40	1.47	2.64	25.5
AS/PMMA	2.18	4.10	1.88	-3.36	36.1
MS/PMMA	2.05	3.10	1.51	2.02	15.2

**Table 3.**  
The roughness parameters of CS/PMMA nanocomposites.

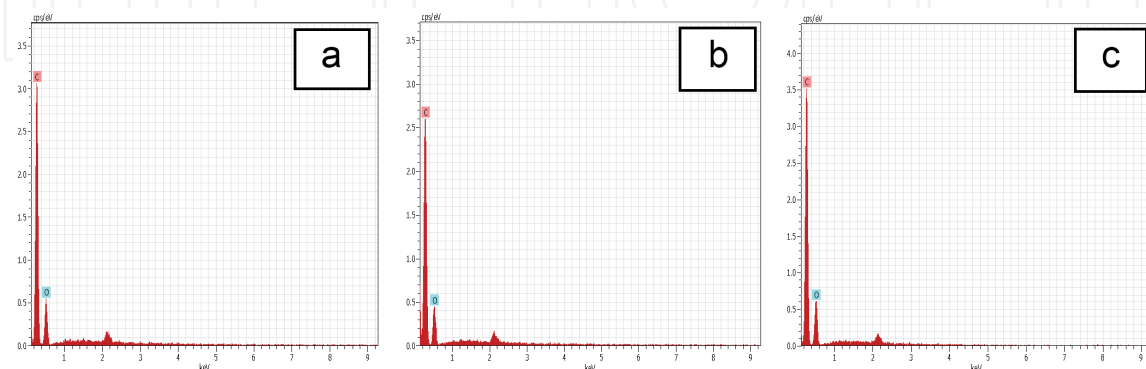


**Figure 16.**  
EDAX spectra of (a) PMMA, (b) almond soot/PMMA, and (c) mustard soot/PMMA samples.

The doping level of almond soot and mustard soot fillers is 1 and 2 mg, respectively. Two broad peaks are centered at  $1725$  and  $1141\text{ cm}^{-1}$  in AS/PMMA and MS/PMMA.

The other peaks are at  $3000$ ,  $2950$ ,  $1440$ ,  $1383$ ,  $1236$ ,  $984$ ,  $839$ ,  $752$  and  $481\text{ cm}^{-1}$ , which correspond to the formation of PMMA matrix. If we compare the pure PMMA and AS/PMMA or MS/PMMA nanocomposites, we will find there is no change in wave number (**Figures 17** and **18**). These show that all AS and MS filler particles were loaded inside the polymer matrix without changing their chemical structure with low intensity as the AS and MS particle concentration increases.

### 5.3 Optical properties

In this section, we discuss the optical properties of polymethyl methacrylate (PMMA), almond soot/PMMA and mustard soot/PMMA nanocomposites for different concentration. The absorbance spectra of nanocomposite thin films were recorded in the range between 200 and 800 nm.

#### 5.3.1 Absorption data

The recorded absorbance spectra of pure PMMA and almond soot (**Figure 19a**) and pure PMMA and mustard soot (**Figure 19b**) nanocomposites with different concentration at the wavelength of 200–800 nm show that the absorbance value increases with the addition of increased carbon soot (AS/MS) nanofillers.

As the absorption peaks increase, these show the existence of internal chemical interaction between the carbon soot nanofillers and PMMA matrix. In this manner, our study of optical properties for PMMA and doped freshly carbon soots such as almond soot particles and mustard soot particles at a different concentration give us good results. The result from synthesized carbon aggregates and aerosol particles

Samples	Elemental compositions	
	C%	O%
Pure PMMA	76.31	23.69
AS/PMMA	76.20	23.80
MS/PMMA	75.26	24.74

**Table 4.**  
 Elemental compositions of PMMA, AS/PMMA and MS/PMMA.

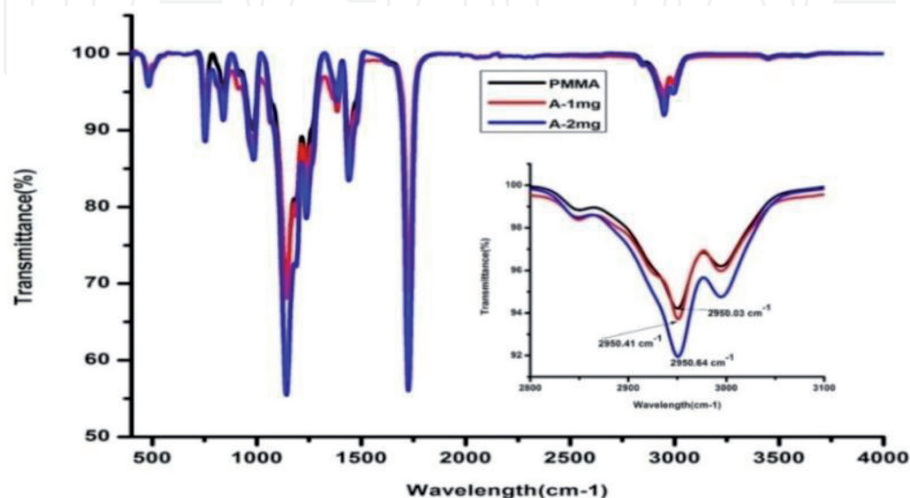


**Figure 17.**  
 The FTIR spectra of pure PMMA and AS/PMMA nanocomposites.

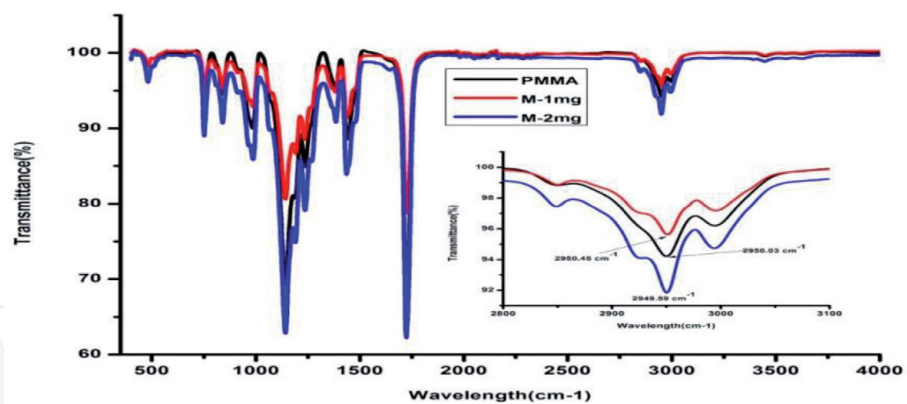


**Figure 18.**  
 The FTIR spectra of pure PMMA and MS/PMMA nanocomposites.

investigated by light scattering and light absorption shows a good agreement with results obtained by other research groups [43, 44].

### 5.3.2 Absorption coefficient data analysis

The absorbance coefficients of PMMA, AS/PMMA (**Figure 20a**) and PMMA, MS/PMMA (**Figure 20b**) nanocomposite thin films are shown in the below figure.

According to a review, if the value of  $\alpha$  is high or  $\alpha > 10^4 \text{ cm}^{-1}$ , then the electron direct transition is expected. If the value of  $\alpha$  is low or  $\alpha < 10^4 \text{ cm}^{-1}$ , then the expected transition of electron is indirect. In our study, the absorption coefficient ( $\alpha$ ) values of the polymer matrix (PMMA) and all filler nanocomposites

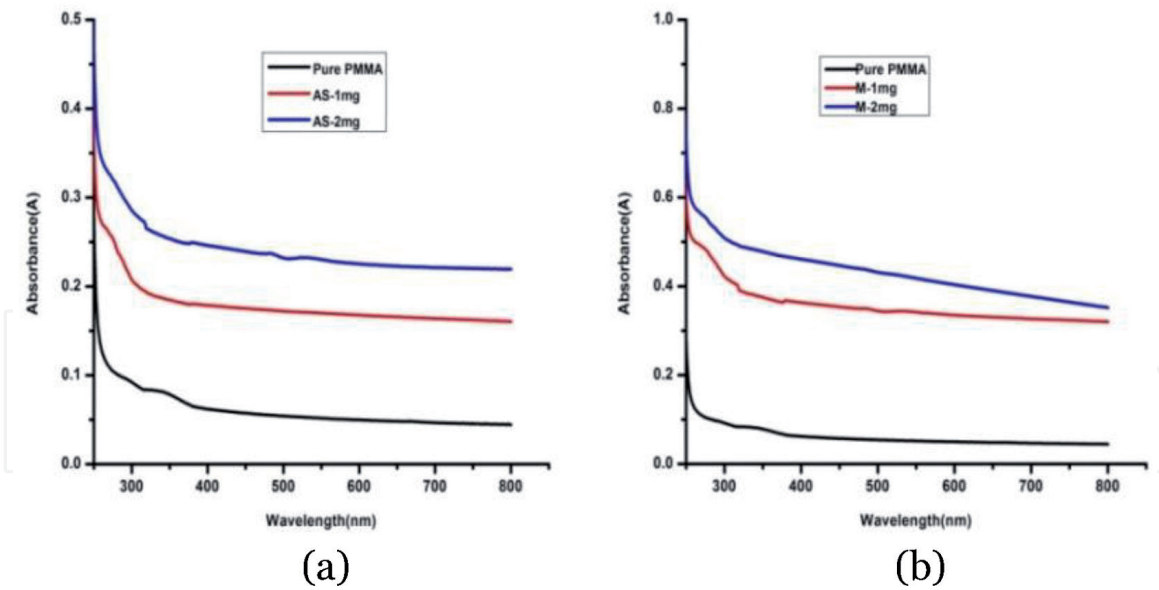


**Figure 19.** Absorbance spectra of pure PMMA with (a) AS/PMMA nanocomposites and (b) MS/PMMA nanocomposites.

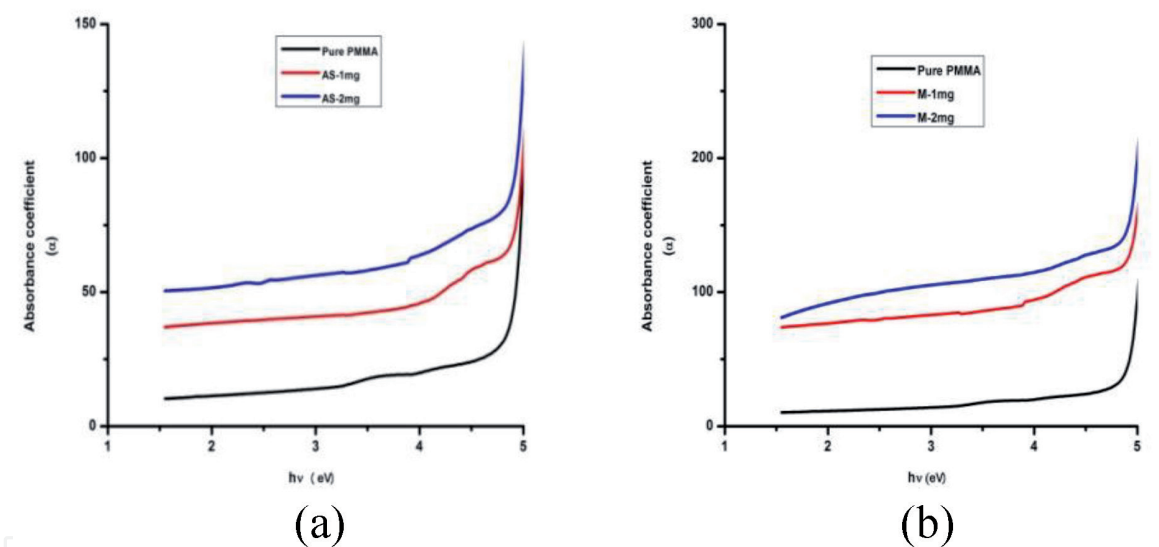


**Figure 20.** Variation of absorption coefficient of PMMA with (a) AS-doped PMMA nanocomposite thin films and (b) MS-doped PMMA nanocomposite thin films.

are not  $>10^4 \text{ cm}^{-1}$ , and this implies the indirect electron transition in AS and MS conditions.

In this study of nanocomposite optical properties, we used carbon nanosoot obtained from incomplete combustion of flame deposition method similar to “Sara D.” et al. in 2018. They found the absorption coefficient for two different flame-generated soot particles, in which the results for both cases were identical [45]. The results of absorbance coefficient for PMMA matrix and carbon soots-doped PMMA nanocomposites indicate indirect electron transition.

### 5.3.3 Band gap analysis

The band gap plots of polymer matrix and AS/PMMA (**Figure 21a**) and polymer matrix and MS/PMMA (**Figure 21b**) nanocomposites on the variation of  $(\alpha h\nu)^{1/2}$  and  $(h\nu)$  are represented. These band gap spectra show that the measurements

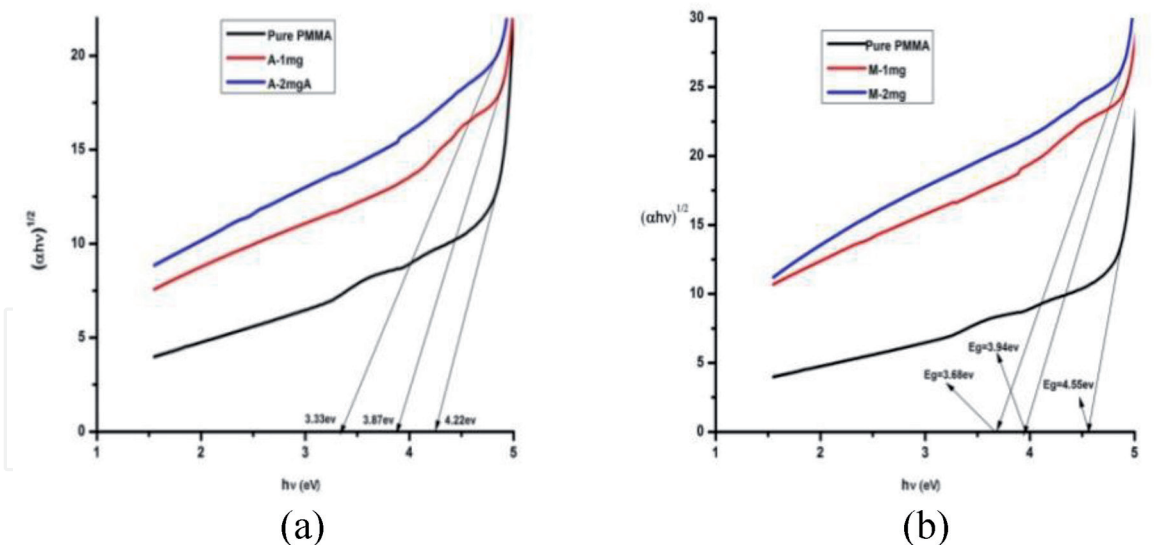


**Figure 21.**  
 The band gap spectra of PMMA with (a) AS/PMMA thin films and (b) MS/PMMA thin films.

Samples	Energy band gap values $E_g$ (eV)
Pure PMMA for AS	4.22
AS-1 mg/PMMA	3.87
AS-2 mg/PMMA	3.68
Pure PMMA for MS	4.55
MS-1 mg/PMMA	3.94
MS-2 mg/PMMA	3.68

**Table 5.**  
 Energy band gap values of PMMA, almond soot and mustard soot nanocomposites.

revealed that the concentration of filler nanoparticles affects the optical properties of PMMA matrix. The decreasing values of optical energy band gap with adding the carbon soot in PMMA, are located in **Table 5**.

## 6. Production of carbon soot (AS and MS)/PS nanocomposites

In this study, we have prepared the polymeric thin film of host matrix PS and carbon soot-doped PS nanocomposites at a different weight percentage of almond and mustard soot of 50  $\mu\text{m}$  thickness by solution casting technique.

The steps for preparation of CS/PS nanocomposite thin films are similar as discussed above in Section 4.

## 7. Properties of CS/PS nanocomposites (CSPNCs)

### 7.1 Surface morphological and chemical composition properties

We measure the surface topology and roughness of CS/PS composites with horizontal length scale in micrometer and vertical scale in the range of nanometer (**Figure 22a–c**).

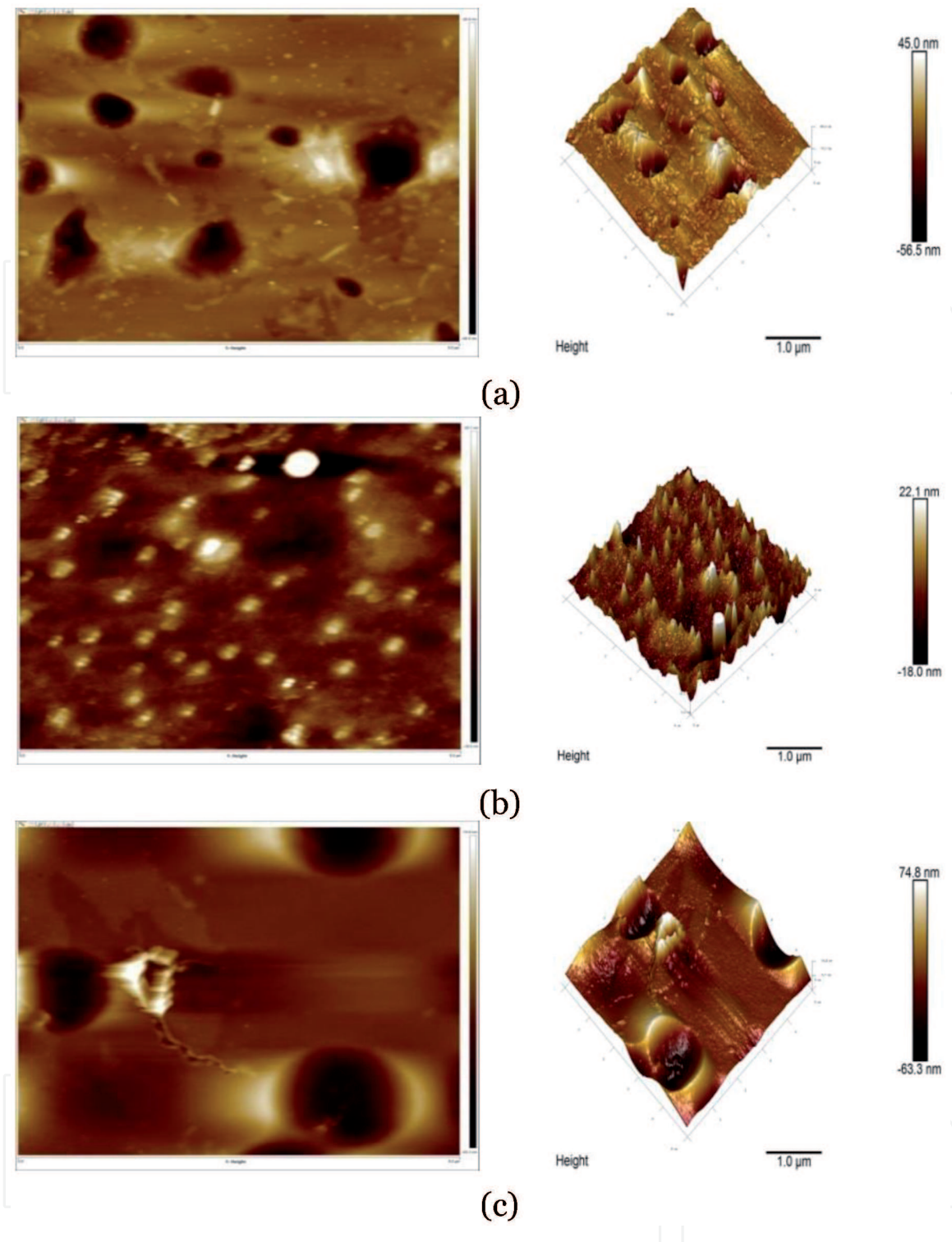


**Figure 22.** Topographic deflection image and 3D AFM image of (a) PS (pure polystyrene), (b) AS/PS nanocomposite thin film and (c) MS/PS nanocomposite thin film.

The roughness parameters of carbon soot polymer nanocomposites (CSPNCs) including the average surface roughness ( $R_a$ ), root mean square roughness ( $R_q$ ), skewness of the line ( $R_{sk}$ ) and kurtosis of the line ( $R_{ku}$ ) roughness are obtained by AFM machine. The average surface roughness for pure PS, AS/PS and MS/PS with values of 2.99, 2.18 and 2.05 nm is carried out as well as the root mean square roughness for pure PS, AS/PS and MS/PS nanocomposites with the values of 4.40, 4.10 and 3.10 nm is obtained. Also,  $R_{sk}$  and  $R_{ku}$  values of all samples are found out, while the ratios of  $R_q/R_a$  of all samples are calculated for all composites, as shown in **Table 6**.

As mentioned in the table, the surface roughness decreases with the doping of almond soot in PS matrix and the surface roughness increases with the doping of mustard soot in PS matrix, as compared with the pure polystyrene sample. The obtained result reveals that surface of AS/PS nanocomposites is smoother as compares to that of MS/PS and pure PS sample. We calculated the ratio of root mean square roughness and average roughness, and the ratio of  $R_q/R_a$  almost matched the value of theoretical ratio data. The surface roughness of composite samples plays an important role in the wetting properties.

The analytical composition of soot filler nanocomposites carried out by energy dispersive X-ray spectroscopy of studied samples is represented in **Figure 23a–c**. We can see that all samples contained approximately 98–99% carbon and remaining 1–2% oxygen element (**Table 7**).

It is confirmed that the sample composed of only carbon and oxygen element, without any other element. These CS (AS and MS)/PS samples are electrically non-conducting, and for EDAX analysis, these samples are coated with gold to convert them into electrically conducting. Due to of this, an extra small peak is observed for gold at approximately 2 keV in EDAX spectra (**Figure 23**).

## 7.2 X-ray diffraction properties

The XRD spectra of pure polystyrene almond soot/PS (**Figure 24a**) and mustard soot/PS (**Figure 24b**) nanocomposites at different weight concentration (1 and 2 wt%) are in the range of  $2\theta = 20-90^\circ$ . The X-ray diffraction pattern from pure PS, AS/PS nanocomposites with 1 and 2 wt% and MS/PS nanocomposites with 1 and 2 wt% concentrations does not show any visible peaks. This corresponds to the pure amorphous polymeric structure without any peak and suggested that the carbon soot particles had been exfoliated in the soot nanocomposites, as referred in [46, 47]. As shown in **Figure 24a** and **b**, the XRD pattern of AS/PS and MS/PS nanocomposites at different weight concentrations does not loss own nature. All results suggest that the variation of intensity confirms the presence of carbon soot in polymer nanocomposites.

## 7.3 Spectroscopic properties

The FTIR pattern of pure polystyrene shown as a broad intense peak at  $694\text{ cm}^{-1}$  is attributed to the (C–H) bend due to the ring deformation vibration. A peak at  $2918\text{ cm}^{-1}$  is attributed to C–H stretching with asymmetric  $\text{CH}_3$  group and C=O stretching around  $1739\text{ cm}^{-1}$ .

The two peaks at  $1600$  and  $1491\text{ cm}^{-1}$  are assigned due to aromatic C=C stretching, and the other two peaks at  $1450$  and  $1366\text{ cm}^{-1}$  are attributed to the ester carbonyl stretching vibration and C–H bending vibration. Some bands at  $1216$ ,  $1027$  and  $905\text{ cm}^{-1}$  in the range  $600-1200\text{ cm}^{-1}$  correspond to the plane deformation of

Samples	Surface roughness parameters				
	$R_a$ (nm)	$R_q$ (nm)	$R_q/R_a$	$R_{sk}$	$R_{ku}$
Pure PS	6.69	11.0	1.64	-1.22	8.44
AS/PS	3.53	5.50	1.55	2.61	25.6
MS/PS	10.3	16.3	1.58	0.65	6.67

**Table 6.**  
 The surface roughness parameters of carbon soot/polystyrene nanocomposites.

Samples	Percentile compositions	
	C%	O%
Pure PS	99.36	0.64
AS/PS	99.10	0.90
MS/PS	98.87	1.13

**Table 7.**  
Percentage of element compositions of PS, AS/PS and MS/PS thin film.

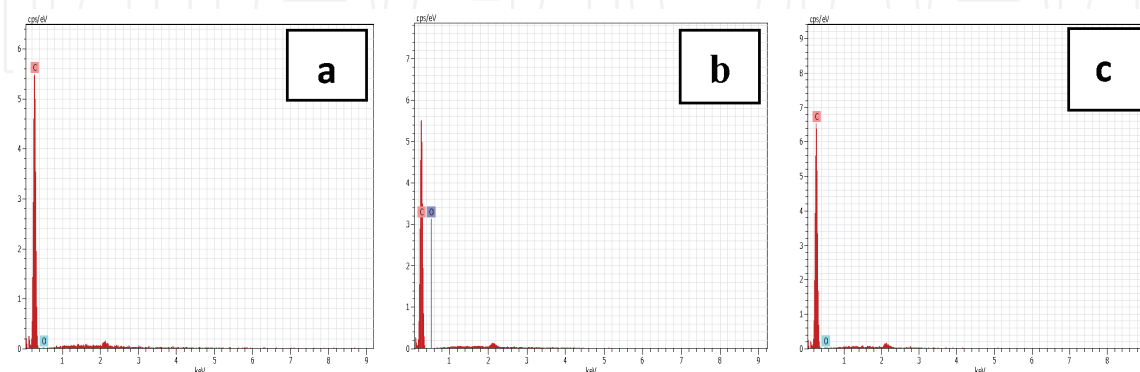


**Figure 23.**  
EDAX spectra of (a) PMMA, (b) almond soot/PMMA and (c) mustard soot/PMMA samples.

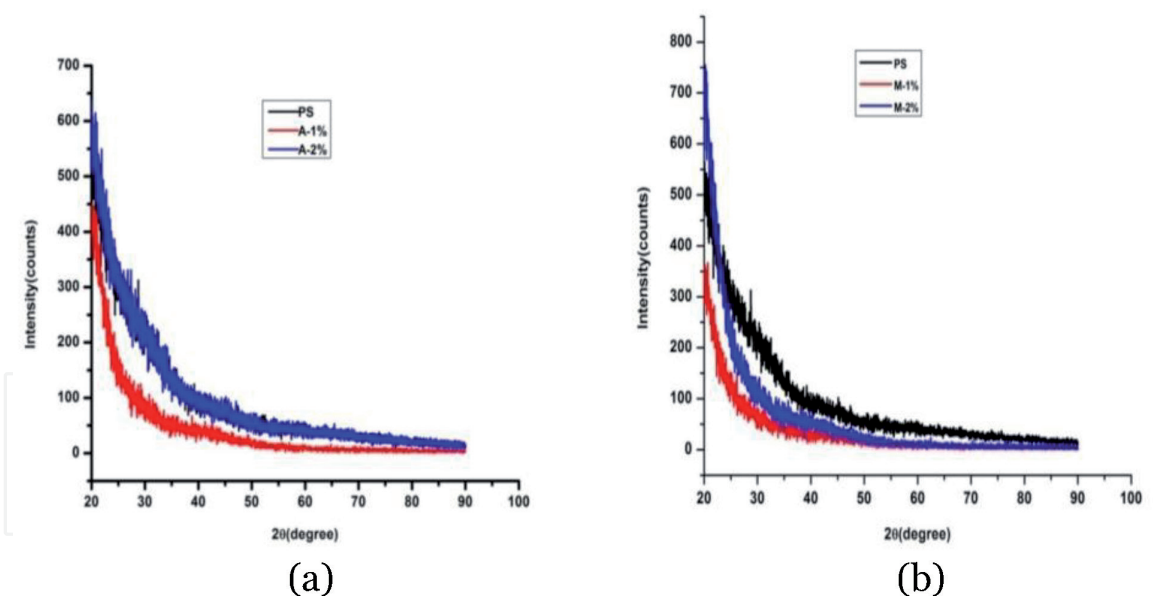


**Figure 24.**  
XRD spectra of (a) almond soot/PS nanocomposites and (b) mustard soot/PS nanocomposites.

C–H group bending. Another peak at  $750\text{ cm}^{-1}$  shows due to (C–H) deformation vibration band of benzene ring hydrogen.

The comparative study on Fourier transform infrared spectra of pure polystyrene vs doped carbon soot/PS nanocomposites shows (Figures 25 and 26) the peaks around  $2920, 1739, 1600, 1492, 1451, 1367, 1215, 1027, 905, 750$  and  $537\text{ cm}^{-1}$  corresponding to the formation of PS. Bands of CS/PS nanocomposites are more and less as compared to the peaks of pure polystyrene, but there are no other peaks found, showing that all the soot nanoparticles are loaded inside the PS host matrix without changing their chemical structure. No other modification in the shift of chemicals

and the shape of band is noticed in the carbon soot/polystyrene nanocomposite spectra, indicating no chemical modification occurred in the polystyrene.

## 7.4 Optical properties

In this section, we discuss about the optical properties of polystyrene nanocomposites. Here, the carbon soot was doped with either almond soot or mustard soot particles with 1 and 2 wt%, respectively. In the optical properties, we tried to understand the absorption coefficient properties. Therefore, we measured the band gap of nanocomposites in the range of 200–800 nm.

### 7.4.1 The absorption data

The absorbance data spectra of pure polystyrene and AS/PS (**Figure 27a**) and pure polystyrene and MS/PS (**Figure 27b**) nanocomposite thin films show the value of absorbance increases with doping the carbon soot in PS as compared to the pure PS. The increased absorbance in spectral profile from nanocomposite reveals the correlation between carbon soot nanoparticles and the host matrix polystyrene matrix. In this study, carbon soot (traditional Indian name—“Kajal”) is produced by incomplete combustion of almond and mustard oil by flame deposition method. Researchers also used different types of soot from aerosol carbon particles, diesel soot and other sources. Similar results were found by Mita et al. in 1980 [48] from absorbance of aerosol soot particles. As seen in the figures, the value of absorbance is low at high wavelength and high absorbance value corresponding to the low wavelengths.

### 7.4.2 Absorption coefficient and band gap study

The absorption coefficient spectra of polystyrene and soot/polymer nanocomposites are represented in **Figure 28a** and **b**.

For the indirect band gap, the value of  $r$  is  $1/2$ ; hence, the indirect band gap of nanocomposite thin films is obtained using the help of plot  $(\alpha h\nu)^{1/2}$  Vs  $h\nu$  (**Figure 29a** and **b**). It has been noticed that the band gap is inversely proportional

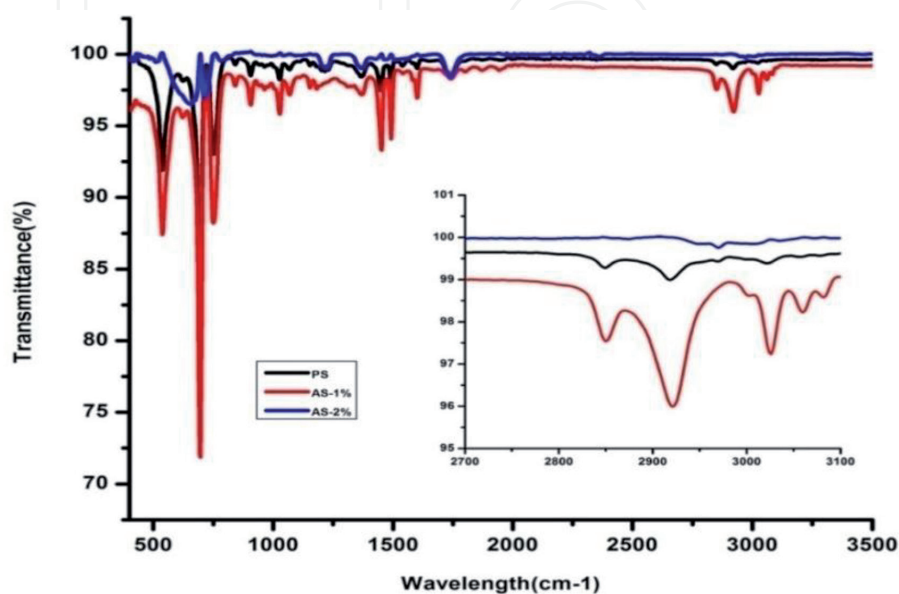


**Figure 25.**  
FTIR spectra of almond soot polystyrene nanocomposites.

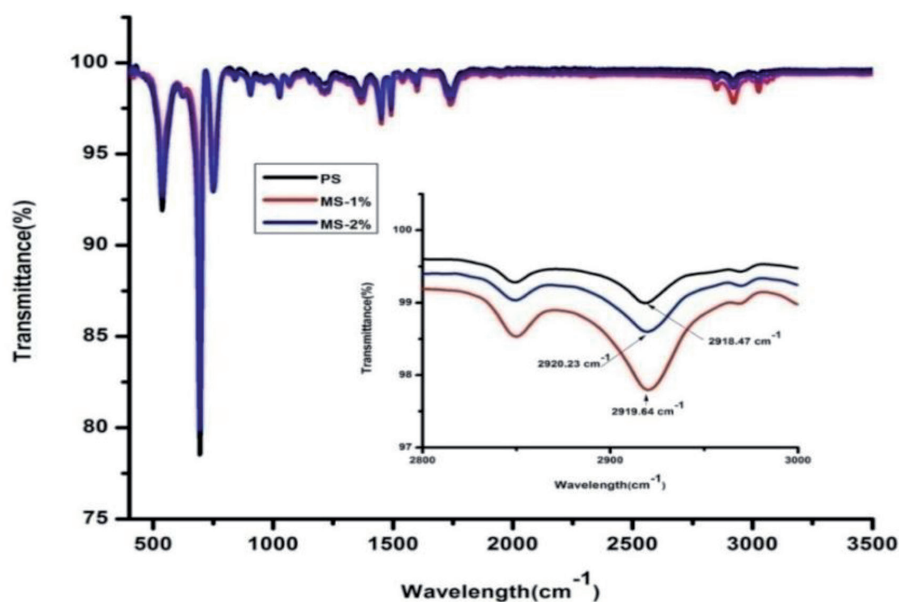


**Figure 26.**  
FTIR spectra of mustard soot polystyrene nanocomposites.

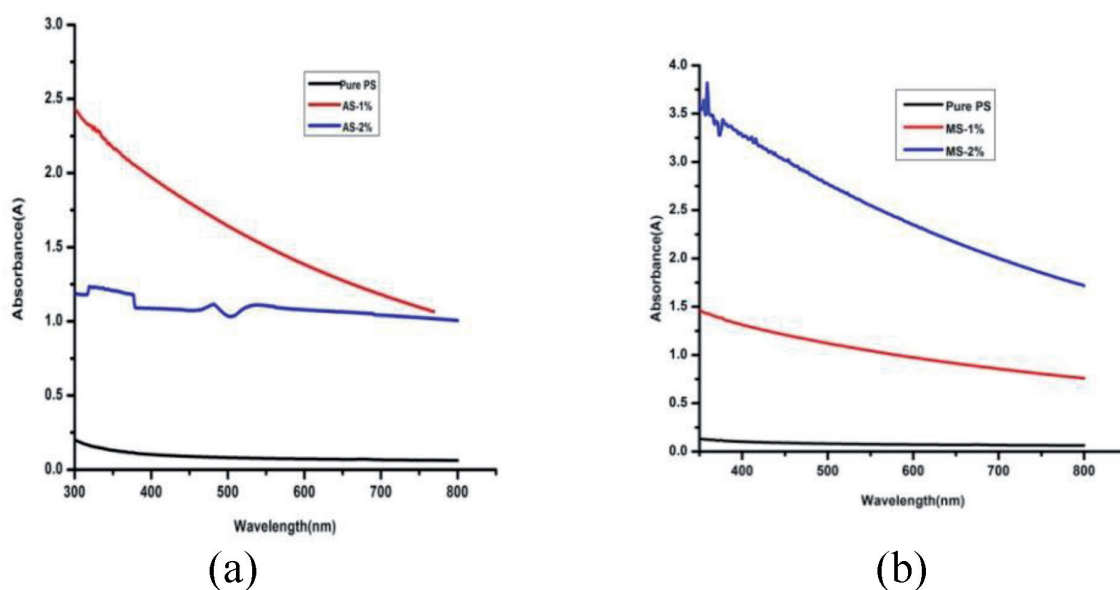


**Figure 27.**  
The absorbance data spectra of pure polystyrene with (a) almond soot-doped PS thin films and (b) mustard soot-doped PS thin films.

to the thickness of films. The indirect band gap of pure PS and AS/PS at 1 and 2 wt% is 4.06 eV, 3.84 and 3.47 eV, as well as for PS, MS/PS at 1 wt% and MS/PS at 2 wt%, it is 4.33, 3.94 and 3.85 eV. Energy band gap values for all thin film samples of 50  $\mu\text{m}$  thickness are represented in **Table 8**.

### 7.5 Glass transition temperature phenomenon ( $T_g$ )

Dynamic mechanical analysis is an amazing tool to study the viscoelastic properties of carbon soot particles filled with polymer. The other authors investigated the mechanical properties of carbon nanoparticles with polymer [48–53]. The dynamical mechanical results of carbon soot/polystyrene nanocomposites produced by solution casting method for pure polystyrene, almond soot/polystyrene and mustard soot/polystyrene at 1 and 2 wt% concentrations (**Figure 30**) show

that for all CS/PS nanocomposites there is a downshift in viscous modulus toward a higher temperature compared to the pure polystyrene. All data were recorded at 1 Hz frequency and 22–160°C temperature.

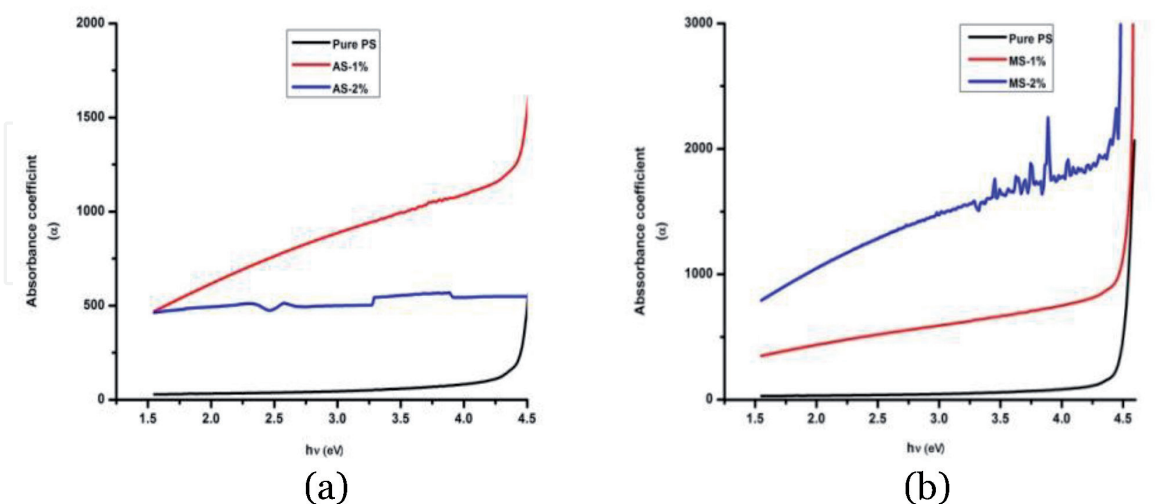


**Figure 28.** Representation of absorption coefficient spectra of pure polystyrene with (a) AS/PS composite for 1 and 2 wt% concentration and (b) MS/PS composite for 1 and 2 wt% concentration.

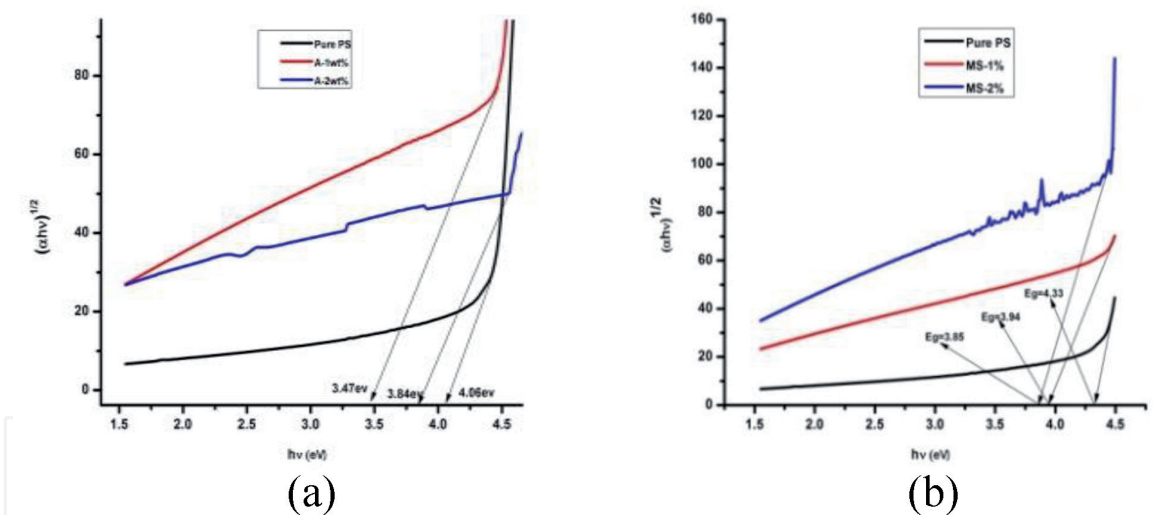


**Figure 29.** Plot of  $(\alpha h\nu)^{1/2}$  vs  $h\nu$  photon energy ( $h\nu$ ) for the pure polystyrene with (a) almond soot 1 and 2 wt% in PS and (b) mustard soot 1 and 2 wt% in PS.

PS and CSPNC samples	Energy band gap $E_g$ (eV)
Pure PS for AS samples	4.06
AS-1 wt%	3.84
AS-2 wt%	3.47
Pure PS for MS samples	4.33
MS-1 wt%	3.94
MS-2 wt%	3.85

**Table 8.** The obtained value of pure polystyrene energy band gap and AS/PS and MS/PS at 1 and 2 wt% concentration.

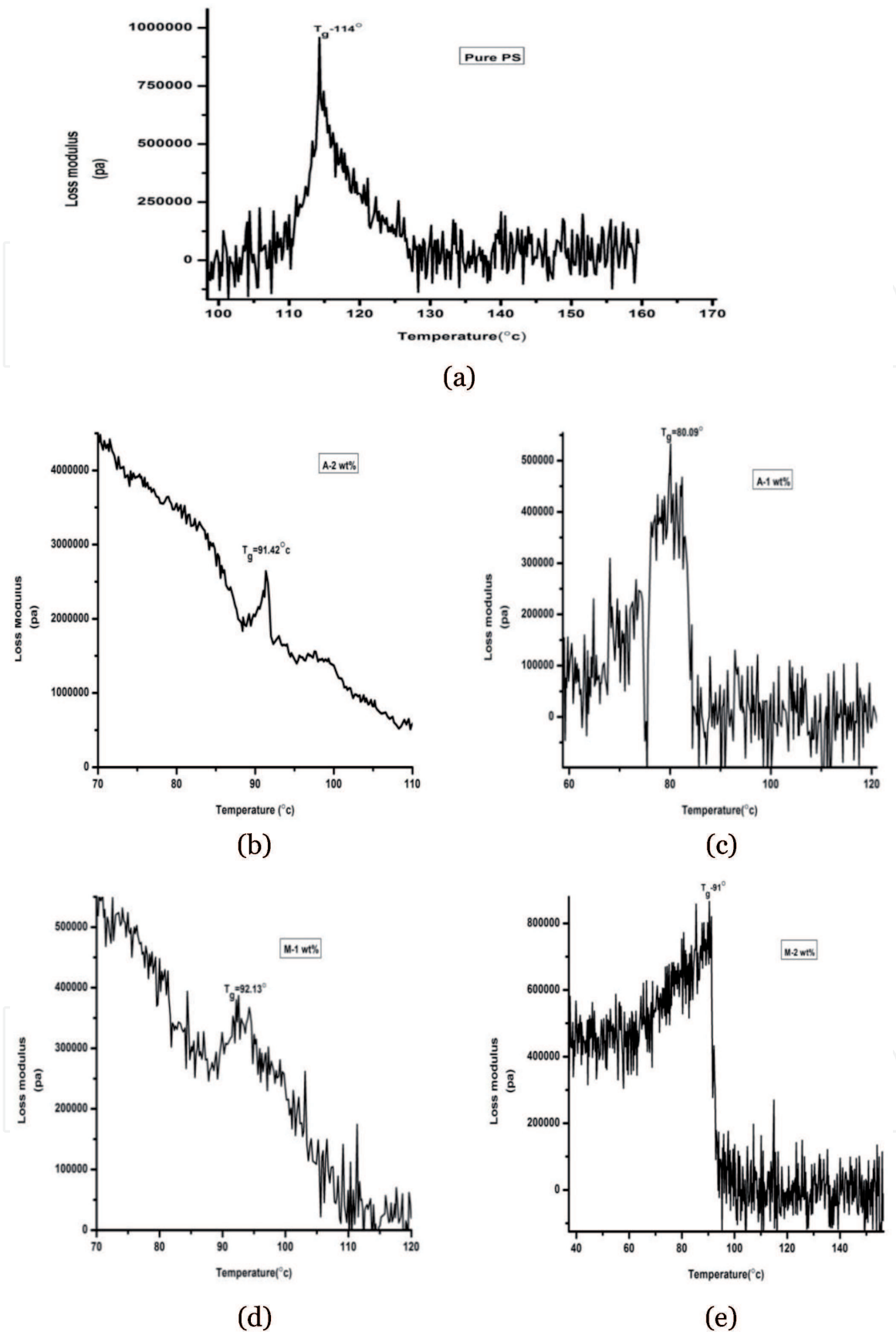


**Figure 30.** Variations of viscous modules ( $E''$ ) with temperature for (a) pure polystyrene, (b) almond-1 wt%/PS, (c) almond-2 wt%/PS, (d) mustard-1 wt% PS and (e) mustard-2 wt%/PS.

The glass transition temperature ( $T_g$ ) of pure polystyrene is  $114^\circ\text{C}$ , and glass transition temperatures for almond soot/PS nanocomposites for 1 and 2 wt% are 80 and  $91^\circ\text{C}$ , as well as for mustard soot/PS nanocomposites at 1 and 2 wt% concentration are 92 and  $91^\circ\text{C}$  (**Table 9**). We can see that the value of glass transition

Samples	Glass transition temperature $T_g$ (°C)
Pure PS	114
A-1 wt%	80
A-2 wt%	91
M-1 wt%	92
M-2 wt%	91

**Table 9.**  
*The glass transition temperature ( $T_g$ ) values of CS/PS nanocomposites.*

temperature decreases for all samples as compared to the pure polystyrene. In the case of AS/PS nanocomposites, the value of  $T_g$  increases with the concentration of almond soot nanoparticles and reveals that the addition of more soot particles hinders the segmental relaxation of the polystyrene chains, while for the MS/PS nanocomposites, the value of  $T_g$  slightly decreases with the increase of mustard soot nanoparticles.

## 8. Conclusions and future scopes

### 8.1 Conclusions

The chapter is concerned with two things: first with carbon soot nanoparticles (CSNPs) and second is carbon soot polymer nanocomposites (CSPNCs). The morphological and spectroscopic analysis is carried out for carbon soot nanoparticles, and the glass transition temperature phenomenon, and optical and structural properties are obtained for the synthesized carbon soot polymer nanocomposites.

Production of carbon soot from incomplete combustion of almond oil and mustard oil by low cost flame deposition method in two different environment one is natural environment (without water tub) and other one is with water tub, these prepared fresh carbon soots such as almond soot (AS) and mustard soot (MS) are characterized by FESEM, XRD, EDAX, FTIR and UV for morphological, elemental composition and spectroscopic analysis. The formed carbon soot particles are the amorphous nanomaterial with the size of approximately 50 nm, confirmed by the XRD and FESEM study. The IR study is carried out to identify the presence of any functional group, some small  $SP^2$ ,  $SP^3$  and aromatic clusters. Here, with water tub condition is an important tool for identifying the morphology and particle size of carbon nanoparticles (CNPs). The synthesized soot is useful for die purpose, paint, marker pen ink, etc. It is also used for pigment and reinforcement in vehicle tires as it decreases the thermal damage.

In the next step, we produced the carbon soot polymer nanocomposites (CSPNCs) for different carbon soot nanoparticles such as almond soot and mustard soot with different polymer matrices of polymethyl methacrylate (PMMA) and polystyrene (PS).

Primarily, we synthesized carbon soot/PMMA nanocomposites with different concentration 1 and 2 mg of AS and MS of 100  $\mu\text{m}$  thickness by solution casting technique. Prepared samples are characterized for the optical and surface morphological properties. FESEM and EDAX provide the useful information about the nanostructure and compositions of nanocomposite samples. FTIR analysis of CS/PMMA nanocomposites shows that the soot nanoparticles are loaded in polymer (PMMA) without change in chemical structure for the surface morphology calculating the surface roughness of all samples, and the decreasing values of

surface roughness with the doping of soot nanoparticles in host matrix PMMA are obtained. In this sequence, the band gap of PMMA and all CS/PMMA nanocomposites are calculated for the optical properties. The lower values of energy band gap are carried out by filling CS in PMMA as compared to the pure PMMA.

For the second case of carbon soot polymer nanocomposites, carbon soot/PS nanocomposites were produced with 1 and 2 wt% concentration of AS and MS nanofillers in host matrix polystyrene by cost-effective solution cast method of 50  $\mu\text{m}$  thickness. The glass transition temperature phenomenon, optical, structural and surface morphological studies are carried out for prepared composite samples. X-ray diffraction study reveals the variation of intensity showing the presence of carbon soot in the polystyrene chain and gives the important information about the amorphous nature. The decreasing values of roughness and band gap are obtained with the doping of carbon soot nanoparticles in the host polymer matrix polystyrene, and also the low values of glass transition temperature  $T_g$  of CS/PS samples are obtained as compared to the pure PS sample. These obtained properties of carbon soot polymer nanocomposites make them very useful in various applications including in the separation of oil and water, anti-icing and energy-saving buildings, high-energy vehicles, electric trains and electric devices.

## **8.2 Future scope**

The incomplete combustion synthesis of carbon soot is a relatively new field of research that has not yet been exploited in all its potentiality. A good controlled incomplete combustion process is flame deposition has represented to be able to synthesis of different carbonaceous particles from burning different oils in a low temperature range. This study provide a deep knowledge of the soot species production method under a flame environment. It was carried out on the experimental results basis. A good relationship between production/combustion conditions and carbon properties like morphological, chemical composition, spectroscopic and internal structure has been found. We can produce the soot by any other method.

Nevertheless, the main focus on investigation of carbon allotropes such as graphine, carbon nanotube (CNT), fullerenes etc by flame deposition method for more demanding applications. Ultimately, the synthesized soot particles through combustion are suitable for industrial applications.

Carbon soot nanoparticles in PMMA and PS could be improved if these nanoparticles are functionalized by some surfactants, and this will be a more homogeneous dispersion of nanoparticles in polymers. Thin films of CS/PMMA or PS could also be casted by spin coating technique. Mechanical and optical properties of CS/polymer samples give faithful results; we can investigate the di-electric and thermal conductivity for further industrial applications.

## **Conflict of interest**

The authors declare no conflict of interest.

## **Abbreviations**

AFM	atomic force microscopy
AS	almond soot
CNPs	carbon nanoparticles
CNTs	carbon nanotubes

CS	carbon soot
CSPNCs	carbon soot polymer nanocomposites
DMA	dynamic mechanical analyzer
EDAX	energy dispersive X-ray
FESEM	field emission scanning electron microscopy
FTIR	Fourier transform infrared spectroscopy
PMMA	polymethyl methacrylate
PS	polystyrene
UV	ultraviolet
XRD	X-ray diffraction

IntechOpen

### **Author details**

Rakhi Tailor\*, Yogesh Kumar Vijay and Minal Bafna  
Vivekananda Global University, Jaipur, India

\*Address all correspondence to: [rrtrbt@yahoo.com](mailto:rrtrbt@yahoo.com)

### **IntechOpen**

© 2020 The Author(s). Licensee IntechOpen. This chapter is distributed under the terms of the Creative Commons Attribution License (<http://creativecommons.org/licenses/by/3.0>), which permits unrestricted use, distribution, and reproduction in any medium, provided the original work is properly cited. 

## References

- [1] Whelan P. The mechanics of the formation and adhesion of deposits arising from the combustion of liquid fuels. The Institution of Mechanical Engineers. 1961:1-17
- [2] Glassman I. Combustion. New York (London): Academic Press; 1977. p. 242
- [3] Grisdale R. The formation of black carbon. Journal of Applied Physics. 1953;24:1082
- [4] Koylu U, Faeth G, Farias TL, Carvalho M. Fractal and projected structure properties of soot aggregates. Combustion and Flame. 1995;100:621-633
- [5] Jensen K, Suo-Antilla J, Blevins L. Characterization of soot properties in two meter JB-8 pool fires. In: Technical Report 2005-0337. California: Sandia National Laboratories; 2005
- [6] Eliot R. Boiler Fuel Additives for Pollution Reduction and Energy Saving. New Jersey: Noyes Data Corporation; 1978. p. 8
- [7] Lindsey A. The formation of polycyclic aromatic hydrocarbons carbon deposits from normal and reversed diffusion flames. Combustion and Flame. 1960;4:261-264
- [8] Seinfeld J, Pandis S. Atmospheric Chemistry and Physics: From Air Pollution to Climate Change. New York: Wiley Interscience; 1997
- [9] Lynn M. Soot diagnostics based on laser heating. Applied Optics. 1984;23:2201-2208
- [10] Joyce D. The life cycle of a debris particle. Tribology and Interface Engineering Series. 2005;48:681-690
- [11] Rocca L, Liberto G, Shayler P, Fay M. The nanostructure of soot in oil particles and agglomerates from an automotive diesel engine. Tribology International. 2013;61:80-87
- [12] Tami C, Robert W. Light absorption by carbonaceous particles: An investigative review. Aerosol Science and Technology. 2006;40:27-67
- [13] Rocca L, Liberto G, Shayler P. Application of nanoparticle tracking analysis platform for the measurement of soot in oil agglomerates from automotive engines. Tribology International. 2014;70:142-147
- [14] Growney D, Mykhaylyk O, Middlemiss L. Is carbon black a suitable model colloidal substrate for diesel soot? Langmuir. 2015;31:10358-10369
- [15] Saito K, Gordon A, Williams F, Stickle W. A study of early history of soot formation in various hydrocarbon diffusion flames. Combustion Science and Technology. 1991;80:103-119
- [16] Megaridis C, Dobbins R. Comparison of soot growth and oxidation in smoking and non-smoking ethylene diffusion flames. Combustion Science and Technology. 1989;66:1-16
- [17] Chen J, Castangoli C, Niksa S. Coal devolatilization during rapid transient heating. Energy and Fuels. 1992;6:264-264
- [18] Haynes B, Wagner H. Soot formation progress. Progress in Energy and Combustion Science. 1981;7:229-273
- [19] Fitzer E, Kocling K, Boetim H, Marsh H. Recommended terminology for the description of carbon as a solid. Pure and Applied Chemistry. 1995;67:473-506
- [20] Bruce C, Stromburg T, Gurton K, Mozer J. Trans spectral absorption

- and scattering of electromagnetic radiation by diesel soot. *Applied Optics*. 1991;**30**:1537-1546
- [21] Desantes J, Bermudez V, Garcia J, Fuentes E. Effects of current engine strategies on the exhaust aerosol particle size distribution from a heavy duty diesel engine. *Journal of Aerosol Science*. 2005;**36**:1251-1276
- [22] Vanderwal R, Tomasek A, Street K, Hull D, Thompson W, Sljenbug J. Carbon nanostructure examined by lattice fringe analysis of high resolution transmission electron microscopy. *Applied Spectroscopy*. 2004;**58**:230-237
- [23] Vandernal R, Tomasek A. Soot oxidation: Dependence upon initial nanostructure. *Combustion and Flame*. 2003;**134**:1-9
- [24] Amann C, Siegl D. Diesel particulates—What they are and why. *Aerosol Science and Technology*. 1982;**1**:73-101
- [25] Esangbedo C, Boehman A, Peres J. Characteristics of diesel engine soot that lead to excessive oil thickening. *Tribology International*. 2011;**47**:194-203
- [26] Clague A, Donnet J, Wang T, Peng J. A comparison of diesel engine soot with carbon black. *Carbon*. 1999;**37**:1553-1565
- [27] Stanmore B, Brillhac J, Gilot P. The oxidation of soot: A review of experiments, mechanism and models. *Carbon*. 2001;**39**:2247-2268
- [28] Sarotim A, Longwell J, Wornat M, Mukherjee J. The role of biaryl reactions in PAH and soot formation. In: *Soot Formation in Combustion*. Springer: Series in Chemical Physics, CHEMICAL; 1994;**59**:485-499
- [29] Tree D, Svensson K. Soot processes in compression ignition engines. *Progress in Energy and Combustion Science*. 2007;**33**:272-309
- [30] Gaydon A, Wolfhard H. *Flames*. London: Chapman and Hall Limited; 1970. pp. 179-180
- [31] Arthur J, Napier D. *Fifth Symposium on Combustion*. London: Chapman and Hall Limited; 1955. p. 303
- [32] Gaydon A, Fairbairn A. *Fifth Symposium on Combustion*. London: Chapman and Hall limited; 1955. p. 24
- [33] Greene E, Taylor R, Patterson W. Mechanism of the pyrolysis of acetylene. *Journal of Physical Chemistry*; 1958;**62**:238
- [34] Dubey P, Muthukumarah D, Dash S, Mukhopadhyay R, Sarkar S. Synthesis and characterization of water soluble carbon nanotubes from mustard soot. *PRAMANA Journal of Physics*. 2005;**65**:681-697
- [35] Baska R, Devashankar S, Sarkar R. Analysis of nano carbon obtained from mustard oil soot. *International Journal of Emerging Technologies in Computational and Applied Sciences*. 2017;**17**:1-5
- [36] Novopashin S, Serebrjakova M, Zaikovoki A. Morphology, chemical composition and magnetization of are discharge Fe–C soot. *Journal of Engineering and Applied Sciences*. 2016;**11**:9130-9133
- [37] Kumar D, Paul E, Kavita K, Singh K, Bhatti H. Synthesis and characterization of water soluble carbon nanotubes. *Journal of Nanoscience*. 2016;**2**:64-65
- [38] Klabunde K. *Nanoscale Materials in Chemistry*. New York: Wiley Interscience; 2001;**1035**:223-262
- [39] Krishnamoorti R, Vaia R. *Polymer nanocomposites: Introduction in polymer nanocomposites synthesis*.

Characterization and hoarding. ACS Symposium. 2002;**804**:1-5

[40] Bandyopadhyay S, Hsieh A, Giannells E. PMMA nanocomposites synthesized by emulsion polymerization. ACS Symposium. 2002;**804**:15-25

[41] Spitaloky Z, Tasis D, Papageli K, Galiotis C. Carbon nanotube polymer composites: Chemistry, processing mechanical and electrical properties. Progress in Polymer Science. 2010;**35**:357-401

[42] Ward H. In: Thomas TR, editor. Rough Surfaces. London: Longman; 1982

[43] Kahnert M, Nousiainen T, Lindquist H, Ebert M. Optical properties of light absorbing carbon aggregates mixed with sulfate assessment of different model geometries for climate forcing calculations. Optical Express. 2012;**20**:10042-10058

[44] Bond T, Bergstrom R. Light absorption by carbonaceous particles: All investigated review. Aerosol Science and Technology. 2006;**40**:27-67

[45] Sara D, Taylor M, Andrew T, Lindsa R, Daniel A, Paola M, et al. Measurement and modeling of the multiwave length optical properties of uncoated flame generated soot. Atmospheric Chemistry and Physics. 2018;**18**:12141-12159

[46] Zhang R, Hu Y, Xu J, Fan W, Chen Z. Flame ability and thermal stability studies of styrene-butmer/graphite oxide nano composite. Polymer Degradation and Stability. 2004;**85**:583-588

[47] Acharya A, Sarwan B, Sharma R, Moghe S, Shrivastav S, Ganesan V. UV-shielding efficiency of TiO<sub>2</sub>-polystyrene thin films prepared by solution cast method. Frontiers

of Physics and Plasma Science- Journal of Physics Conference Series. 2017;**836**:1-5. DOI: 10.1088/1742-6596/836/1/012048

[48] Mita A, Isono K. Effective complex refractive index of atmospheric aerosols containing absorbing substances. Journal of the Meteorological Society of Japan. 1980;**58**:69-78

[49] Sabbar A, Mohammed H, Ibrahim A, Saud H. Thermal and optical properties of polystyrene nanocomposites reinforced with soot. Orientation Journal of Chemistry. 2019;**35**:455-460

[50] Russo C, Stanzione F, Alfe M, Cicyolo A, Tregrossi A. Spectral Analysis in the UV-Visible Range for Revealing the Molecular Forms of Combustion Generated Carbonaceous Species. Italy: Chia Laguna; 2011

[51] Gandhi K, Salovey R. Dynamic mechanical behavior of polymers containing carbon black. Polymer Engineering and Science. 1988;**28**:877-887

[52] Ibarra L, Macais A, Palma E. Viscoelastic properties of short of short carbon fiber thermoplastic (SBS) elastomer composites. Journal of Applied Polymer Science. 1995;**57**:831

[53] Nigrawal A, Chand N. Studies on dynamic mechanical analysis and morphology of carbon soot filled in saturated polyester graded composites. International Journal of Science Engineering and Advance Technology. 2014;**2**:116-119